Journal of Materials Chemistry A

Accepted Manuscript

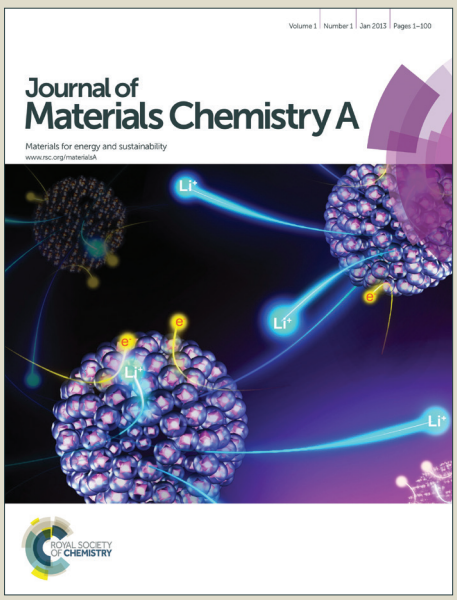

ROYAL SOCIETY OF CHEMISTRY

www.rsc.org/materialsA

Journal of Materials Chemistry A

Dynamic Article Links ►

Cite this: DOI: 10.1039/c0xx00000x

PAPER

www.rsc.org/xxxxxx

Stretchable All-Solid-State Supercapacitor with Wavy Shaped Polyaniline/Graphene Electrode

Yizhu Xie,[a] Yan Liu,[a] Yuda Zhao,[a] Yuen Hong Tsang,[a] Shu Ping Lau,[a] Haitao Huang,[a] Yang Chai*[a,b]

Received (in XXX, XXX) Xth XXXXXXXXX 20XX, Accepted Xth XXXXXXXXX 20XX

DOI: 10.1039/b000000x

Stretchable electronic device can retain the functionalities during high-level mechanical deformation, and stimulates the applications in the field of wearable and bio-implantable electronics. Efficient energy storage devices are an indispensable component in the stretchable electronic systems. To integrate power supplies together with the electronic devices that are mechanically flexible and stretchable, we demonstrate a new kind of stretchable all-solid-state supercapacitor, which consists of two slightly separated polyaniline/graphene electrodes in a wavy shape, and phosphoric acid/polyvinyl alcohol gel as a solid-state electrolyte and separator. The as-fabricated wavy shaped supercapacitor was encapsulated in elastomeric substrate that can be stretched to a large scale without mechanical degradation. The supercapacitor exhibited a maximum specific capacitance of 261 F/g. The electrochemical cycling test of the supercapacitor showed 89% capacitance retention over 1000 charge/discharge cycles at a current density of 1 mA/cm^2. The bending and stretching tests showed that the supercapacitor maintained high mechanical strength and large capacitance simultaneously, even under the strain of 30%. This stretchable all-solid-state supercapacitor shows a high potential as an energy storage device for stretchable electronic system.

1. Introduction

There have been rapid developments towards stretchable electronics to meet the increasing demands in wearable and bio-implantable electronics. A variety of flexible and stretchable devices and systems have been successfully demonstrated, including stretchable light emitting diodes,[1-3] photo-detectors,[4-7] photo-voltaics,[8,9] 'epidermal' health/wellness monitors,[10,11] sensitive robotic skins,[12-14] and electronic compound eye camera.[15] The operation of electronic device usually requires the use of external power supply through cables/wirings, which have to be fixed to a specific location to connect power sources, and greatly hinder the portability. Therefore, embedded power sources are typically used in the stretchable or wearable systems to get rid of the unwieldy wires/cables. It requires researchers to develop stretchable power sources that can accommodate large strains without significantly degraded performance. Among various power-source devices, supercapacitors are currently attracting intensive attention because they can provide energy density higher by orders of magnitude than conventional dielectric capacitors, and larger power density and longer cycling ability than batteries.[16-20] To integrate supercapacitor in a stretchable electronic system, it should accommodate large strains and retain high performance during the mechanical deformation. However, the fabrication of stretchable supercapacitors remains a challenge because it requires the electrode, electrolyte and separator in the supercapacitor to have similar stretchability.

Until now, only few works on stretchable supercapacitor have been reported.[21-25] Yu *et al.*, Li *et al.*, and Niu *et al.* deposited single-walled carbon nanotubes (SWNT) macrofilm on the pre-strained elastomeric substrates, and formed buckled SWNT electrodes to accommodate the deformation of the supercapacitor.[21,23,24] The specific capacitances in these works are relatively low because the SWNT electrode is not a pseudo-capacitive material, and mainly stores energy through the electric double-layer mechanism.[26,27] In addition, the use of pre-strained substrate is incompatible with most of fabrication procedures of other electronic devices.[1-15] To avoid the use of pre-strained substrates that hinder the integration of supercapacitor with other stretchable devices, Kim *et al.* demonstrated a stretchable micro-supercapacitor array interconnected by serpentine metal lines.[25]

[a] *Department of Applied Physics, The Hong Kong Polytechnic University, Hung Hom, Kowloon , Hong Kong, People's Republic of China*
E-mail: ychai@polyu.edu.hk
[b] *The Hong Kong Polytechnic University, Shenzhen Research Institute, Shenzhen, People's Republic of China*

†*Electronic Supplementary Information (ESI) available: [Optical image of wavy shaped Ni foam and Graphene; Electrical resistance variation of the wavy shaped porous graphene as a function of the different stretching statues; SEM images of PANI/graphene prepared by DC electrochemical deposition; SEM images of porous graphene and PANI/graphene prepared by pulsed electrochemical deposition; The CV curves of the PANI/graphene electrode at different scan rates in 1 M H_2SO_4 aqueous electrolyte.] See DOI: 10.1039/b000000x/*

The electrode in this work was also SWNT, and the device showed relatively low specific capacitance. Hu and his co-workers demonstrated stretchable supercapacitor on textile using SWNT electrodes by a simple fabrication process without pre-strain.[22] Furthermore, they increased the specific capacitance by loading pseudo-capacitive MnO_2 to the SWNT electrode. However, the stretchability of the SWNT/MnO_2 electrode was not examined in this work. Later, Xie *et al.* showed that 3D MnO_2/graphene electrode exhibited poor flexibility, and collapsed, cracked easily during bending or stretching operation due to the intrinsic rigidity of MnO_2.[28, 29] Recently, Chen *et al.* reported supercapacitors based on wrinkled graphene electrodes, enabling stretching up to 40%.[30]

Polyaniline (PANI) is a common pseudo-capacitive material for substantially increasing the electrochemical capacitance of the supercapacitor, and has good electrical conductivity, large valence state change during electrochemical reaction, and high mechanical flexibility compared with other inorganic pseudo-capacitive materials, *e. g.* MnO_2. In most of the reported PANI-based supercapacitor works, the form of PANI is usually nanostructured decoration to increase the specific area of the electrode and decrease the diffusion path of the electrolyte.[18,31-37] These nanostructured PANI usually showed poor mechanical strength, and can be ruptured during the mechanical deformation. In contrast, a dense PANI thin film showed improved mechanical strength and can accommodate a large mechanical deformation without failure.[38] Three-dimensional (3D) porous graphene consists of interconnected pore structures, allows the access of electrolyte ions to the internal surface of graphene film, provides large effective specific area, and enables the formation of composite with other pseudo-capacitive materials.[39-42] Unlike SWNT network where presents a large contact resistance between nanotubes, the graphene sheets in 3D porous graphene are chemically bonded together in the growth process, and have lower internal contact resistance.

In order to increase the specific capacitance and maintain the stretchability to a large scale, we show a kind of stretchable all-solid-state supercapacitor with wavy shaped PANI/graphene electrodes. We conformally deposited a dense PANI thin film on the surface of wavy graphene electrode by pulsed electrochemical deposition. The use of both high specific-area graphene and pseudo-capacitive PANI forms a hybrid supercapacitor[43] to increase the electrochemical capacitance. Our supercapacitor show higher specific capacitance than those of stretchable or flexible solid-state SWNT and PANI/SWNT supercapacitors.[24,25,44] The wavy shaped supercapcitor was encapsulated in an elastomeric substrate, exhibiting high flexibility and stretchability. Remarkably, the electrochemical performance of the stretchable supercapacitors almost remained unchanged even under high bending (180°) and 30% tensile strain.

2. Experimental details

2.1 Fabrication of Porous Graphene Sheet in Wavy Shape

Ni foam was used as catalyst for growing porous graphene. First, Ni foam (100 pores per inch, 320 g/m^2 surface density, thickness of ~ 1.5 mm) was cut into pieces of 1×0.25 inch, was pressed into a thin sheet ~ 200 μm thick and then manually made to wavy shape (wavelength of ~ 1.3 mm, amplitube of 0.5 mm) by using a steel rod with the diameter of 0.89 mm. Then the samples were cleaned in 1 M HCl solution for 10 min and in acetone and deionized water for 15 min, respectively. Second, a typical growth process was as follows: (1) The standard 1.5 inch quartz tube was heated in a furnace up to 1000 °C under H_2:Ar gas flow; (2) Ni foam was introduced into the hot-zone of the furnace by moving the quartz tube (under H_2:Ar=1:10, 150 sccm gas flow) and then annealed for 30 min to clean their surfaces and eliminate a thin surface oxide layer; then 10 sccm CH_4 was introduced into the reaction tube under atmospheric pressure for 5 min growth; (3) the Ni foam was quickly cooled down to room temperature under a H_2/Ar atmosphere by quickly pulling it out from the hot-zone of the furnace. Third, the sample were took out from furnace, and then drop-coated with a poly(methylmethacrylate) (PMMA) solution (4.5% in anisole) and baked at 150 °C for 30 minutes. Fourth, these samples were put into a 3 M HCl solution for 24 hours to completely dissolve the Ni foam to obtain the PMMA/graphene. Finally, porous graphene sheet with wavy shape were obtained after removing PMMA in hot acetone at 50 °C.

2.2 Fabrication of PANI /Graphene

Cu wires were embedded and connected to wavy shaped graphene with Ag paste. Aniline monomer (0.1 M, 99.5% Sigma Aldrich) and H_2SO_4 (0.5 M) were used as the plating solution. Proper mixing was ensured via stirring and ultra-sonication. Then pulsed electrodeposition was conducted with the pulse length 4 s for 60 cycles. We controlled the peak current density at 2 mA/cm^2 to ensure that the PANI can be deposited onto the surface of the internal graphene sheet. After the PANI deposition, the resulting material was washed with DI water and dry at 50 °C. Finally, the sample was dried in a vacuum oven at a temperature of 80 °C.

2.3 Fabrication of Stretchable Supercapacitor

First, the H_3PO_4/PVA gel electrolyte was prepared as follows: PVA powder and water (1 g PVA/10 mL H_2O) were mixed and heated to 90 °C under constant stirring until the solution became clear. After cooling the solution down, concentrated H_3PO_4 was added (1 g) and the viscous solution was thoroughly stirred until a clear solution was obtained. Second, PANI/graphene electrode on Ecoflex/glass slide was immersed in the H_3PO_4-PVA aqueous solution for 10 min and picked out. After that, the electrode was dried in air at room temperature for 6 h to vaporize the excess water. Then two identical electrodes were stacked together by coating a uniform layer of H_3PO_4-PVA aqueous solution between them. The gel electrolyte becomes one thin separating layer between the two electrodes. After the solidification of two slightly separated PANI/graphene electrodes with H_3PO_4-PVA gel electrolyte, one supercapacitor device was obtained. The sample is then embedded into Ecoflex aqueous solution and curing.

2.4 Characterization

The morphologies of the obtained structures were characterized by scanning electron microscopy (SEM, JEOL JSM-6490). The Raman spectroscopy of porous graphene and

PANI/graphene was measured by Raman system (HORIBA HR800) with an excitation wavelength of 488 nm. Electrochemical studies (cyclic voltammetry, galvanostatic charge-discharge) were carried out by electrochemical workstation (Shanghai Chenhua 660c). Electrochemical impedance spectroscopy (EIS) was conducted on constant voltage mode by sweeping the frequency from 0.1 Hz to 10 kHz.

3. Results and discussion

Porous graphene can withstand large-scale bending and folding, but will be fractured by high-level stretching. By bending the 3D porous graphene to a wavy shape, this will enable the porous graphene to accommodate the strain without mechanical failure. It is important to evaluate the resistance change of the wavy shaped porous graphene during stretching because it can affect the performance of stretchable supercapacitors. We bent the porous graphene electrode in a shape close to sine wave, as shown in (Supporting Information) Figure S1(a) and (b). The wavelength is ~2.6 mm, and the amplitude is ~0.5 mm. According to the rough calculation of the characteristics of sine wave, we can predict that the wavy shaped graphene can be stretched about 30%. We encapsulated the wavy shaped graphene electrode into elastomeric Ecoflex, and measured the sheet resistance under different strain levels. Figure S2 shows the resistance change of porous graphene electrode as a function of the strain. The resistance change is less than 3% even under 30% strain. This is in contrast with the results reported in the existing literatures, where the stretching induced fracture of the graphene sheet, caused significant resistance change, and can be used for high-sensitive strain sensors.[44,45] In our structure, the stretching can be mainly accommodated by the wavy shape. The graphene sheet is less likely to be fractured in the stretching, resulting negligible resistance change. These results show excellent stretchability of the wavy shaped porous graphene. The stretching level can be further modified by the amplitude and wavelength of the wavy shape.

Figure 1 schematically shows the process flow of fabricating a stretchable supercapacitor with PANI/graphene electrode. First, a piece of flat Ni foam with the thickness of 200 μm (figure 1(a)) was manually made into wavy shape (figure 1(b)). The wavy shaped Ni foam was used as catalyst for growing porous graphene by atmospheric pressure chemical vapor deposition (CVD), and the Ni skeleton was chemically removed by the wet etching in a solution of 3 M HCl. The resulting porous graphene sheets remained wavy shape after the wet etching, as shown in Figure 1(c) and Figure S1. Cu wires were embedded and connected to the wavy shaped graphene sheets with Ag paste, which formed a low-resistance electrical contact between the Cu wires and the graphene sheet. Dense PANI thin films on porous graphene sheets were conformally deposited onto graphene surface by pulsed electrodeposition, as depicted in figure 1(d). Flexible phosphoric acid/polyvinyl alcohol (H_3PO_4-PVA) was used as gel electrolyte as well as a separator in the all-solid-state supercapacitors.[47,48] This solid-state electrolyte is mechanically flexible and avoids the leakage associated with the liquid-state electrolyte. The thickness of the PANI/graphene electrode was reduced to around 100 μm because of the evaporation of the excess water and the shrinking of electrolyte. The two wavy shaped PANI/graphene electrodes were stacked together but separated by a gel electrolyte layer, as shown in Figure 1(e). The as-prepared supercapacitor was encapsulated by Ecoflex, which protects electrode materials and electrolyte from atmosphere and humidity, and provides supporting substrate for the stretchable supercapacitor. Figure 1(f) shows the schematic of the encapsulated wavy shaped supercapacitor into elastomeric Ecoflex.

Figure 2(a) shows the optical images of porous graphene/Ni and graphene sheet. The wavelength and amplitude of the wavy shape almost remain unchanged after the wet etching process.

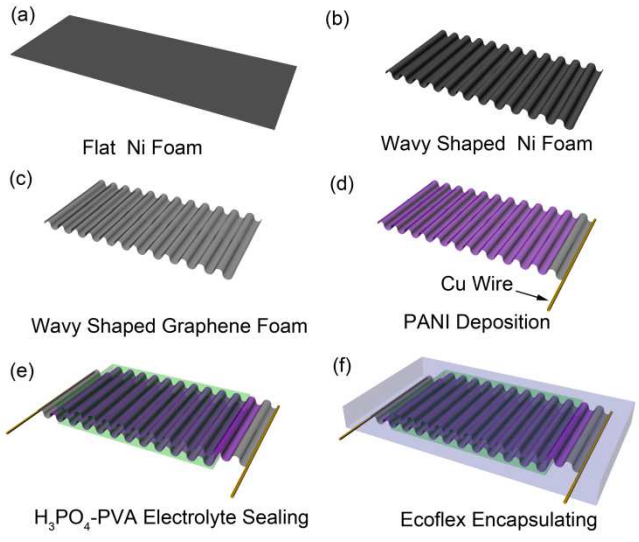

Figure 1. Schematics of fabricating a stretchable supercapacitor. (a) Flat Ni foam (b) Wavy shaped Ni foam. (c) Preparing porous graphene in wave shape by using Ni foam as catalyst. (d) Depositing PANI onto porous graphene by pulsed electrochemical deposition. (e) Coating of H_3PO_4-PVA gel electrolyte. (f) Encapsulating supercapacitor by elastomeric Ecoflex.

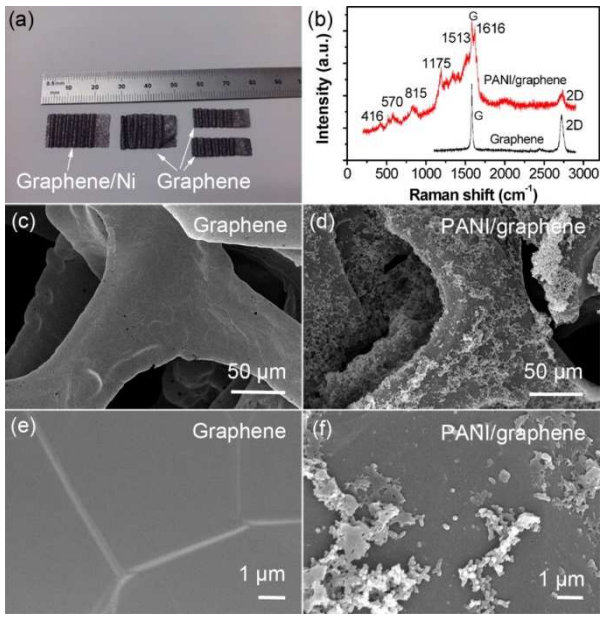

Figure 2. (a) Optical image of the porous graphene/Ni and graphene. (b) Raman spectroscopy of the porous graphene and PANI/graphene. SEM images of (c)(e) porous graphene and (d)(f) PANI/graphene.

Figure 2(b) shows the Raman spectra of the graphene electrodes before and after the PANI deposition. The ratio of G and 2D peak intensity in Raman spectroscopy of the porous graphene is around 1.85, indicating that the graphene is multiple layered. The Raman spectrum shows typical characteristic peaks of PANI.[49,50] The peak of 416 cm^{-1} is indicative of C-N-C out-of-plane deformation mode, the peak of 570 cm^{-1} is related to the deformation mode of protonated amine groups, and the peak of 815 cm^{-1} is a characteristic of a mixture of various torsion angles between the two aniline rings of the PANI structures.[50] The characteristic peaks in the range of 1000-1700 cm^{-1} are related to the PANI oxidation states.[38]

Figures 2(c)-(f) present scanning electron microscopy (SEM) images of the samples before and after the pulsed electrochemical deposition of PANI. Figure 2(c) shows wrinkles and even some cracks in the porous graphene. The wrinkles originate from the surface of Ni foam, which can be seen more clearly from high-magnified SEM image in figure 2(e). The DC electrochemical deposition leaded to the dense PANI coating only on the graphene surface, as shown in the top-view SEM images in Figure S3. The specific area was reduced in this structure, and the electrochemical capacitance is decreased. Thus, we used the pulsed electrochemical deposition for the PANI coating. The samples deposited by 60 pulse cycles show balanced performances between electrochemical capacitances and mechanical strength. The PANI/graphene electrode maintained porous structure and retained high specific area, as shown in the Figure S4. From the enlarged SEM in Figure 2(d) and 2(f), one can observe PANI thin film coated on the surface of porous graphene, and formed PANI nanostructures on top of the PANI thin film. The dense PANI thin film enhances the mechanical strength of the graphene electrode, and the topped PANI nanostructure increases the specific area of the electrode as well as the capacitance of the supercapacitor. Before we integrated the PANI/graphene electrode for all-solid-state supercapacitor, we conducted the electrochemical characterization of the electrode in an aqueous electrolyte (1 M H_2SO_4). Figure S5 shows the cyclic voltammograms (CVs) of the PANI/graphene electrode tested in aqueous solution, presenting the obvious electrochemical redox reaction. H_3PO_4-PVA gel was used in the stretchable solid-state supercapacitor as electrolyte and separator. Figure 3(a) shows the cross-sectional SEM image of the sandwich structure of a PANI/graphene supercapacitor without Ecoflex encapsulation. The total thickness of the all-solid-state supercapacitor is approximate 300 μm with ~100 μm for each PANI/grapheme electrode, and ~100 μm for the intermediate polymer gel

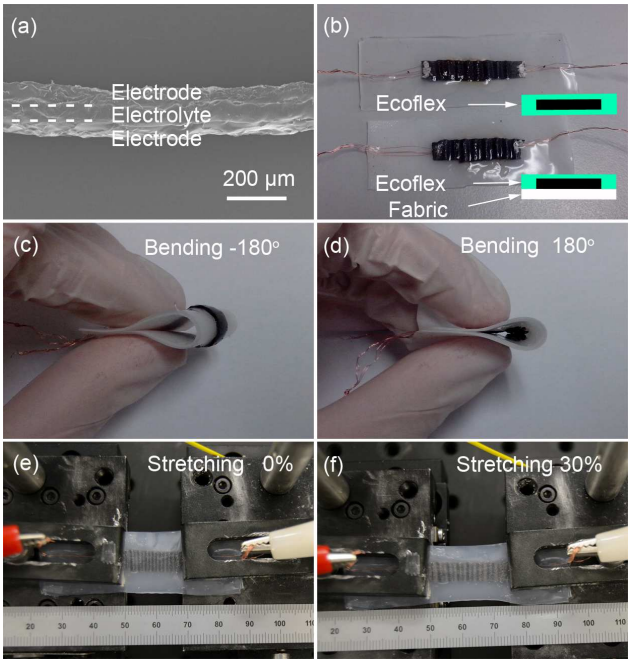

Figure 3. (a) Cross-sectional image of the device. (b) Stretchable supercapacitors encapsulated in Ecoflex and Ecoflex/fabric. Insets are the cross-sectional schematic of the device. Optical images of bent all-solid-state supercapacitor at (c) -180° and (d) 180°. Optical images of stretched all-solid-state supercapacitor under strain of (e) 0% and (f) 30%.

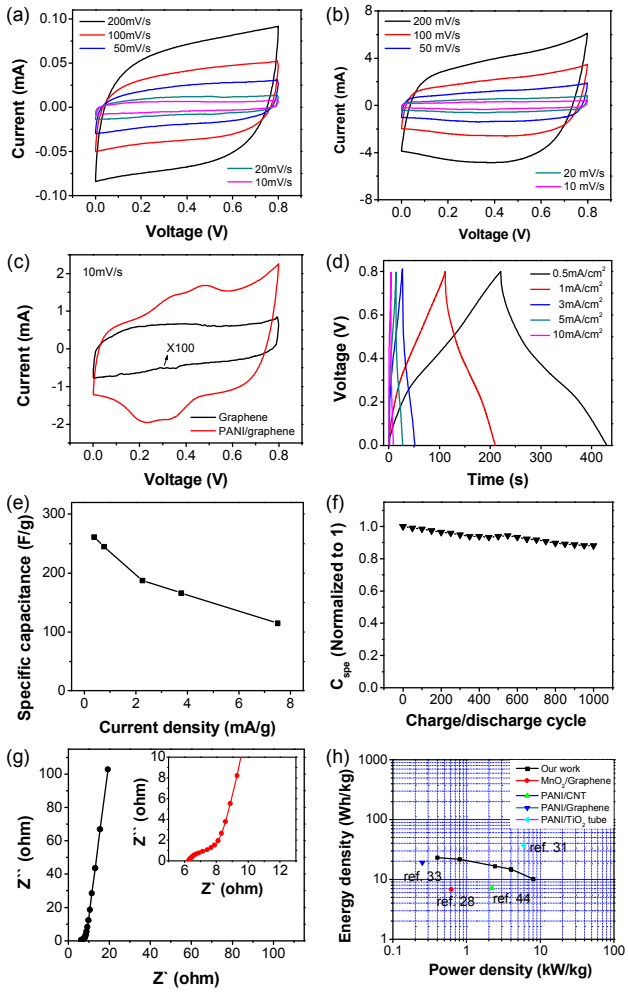

Figure 4. Electrochemical performance of stretchable all-solid-state supercapacitors. The CV curves of the supercapacitor (a) with porous graphene electrodes at different scan rates, (b) with PANI/graphene electrodes at different scan rates, and (c) porous graphene electrode with and without PANI at the scan rate of 10 mV/s. (d) Galvanostatic charge/discharge curves of the stretchable supercapacitor with PANI/graphene electrodes at different current densities. (e) The specific capacitance of the stretchable supercapacitor with PANI/graphene electrodes at different charge/discharge current densities. (f) Cycling performance of the stretchable supercapacitor with PANI/graphene electrodes for charging and discharging at a current density of 1 mA/cm^2. (g) Nyquist plot of the stretchable supercapacitor. (h) Ragone plots of the stretchable supercapacitor with PANI/graphene electrodes.

electrolyte. We encapsulated the as-prepared supercapacitor by Ecoflex. As a proof-of-concept demonstration for the wearable electronics, we also encapsulated the supercapacitor between Ecoflex and fabric, as shown in figure 3(b). Insets of figure 3(b) show the cross-sectional schematic of the all-solid-state supercapacitor structure. Our supercapacitors can be bended from -180° to 180°, and also can be uni-axially stretched up to 30%, as shown in Figure 3(c)-(f). These results clearly showed that our wavy shaped design allows the device to be tolerant of the mechanical deformation to a large scale.

Figure 4(a) shows the CV curves of the all-solid-state supercapacitor with only porous graphene electrode. The shape of the CV curves is rectangular within the selected range of potential (0-0.8 V) even at high scan rate of 200 mV/s, and the current responds to voltage reversal rapidly, indicating the fast diffusion of ions in the electrodes. Figure 4(b) shows the CV curves of the all-solid-state supercapacitor with porous PANI/graphene electrode under the same potential range and different scan rates. Although the shape of these CV curves of PANI/graphene supercapacitor are similar to that with porous graphene electrode, the current response increases by over one hundred times at the same scan rate, which can be seen clearly from the CV curves (Figure 4(c)) of the supercapacitors with and without PANI at the same scan rate of 10 mV/s. The peaks in the CV curve of the PANI/graphene supercapacitor indicate the electrochemical redox reaction resulted from the presence of pseudo-capacitive PANI. Specifically, the peaks are ascribed to the transformation between leucoemeraldine base states and emeraldine salt (ES) states of the PANI, and the transformation between ES and perni-graniline base states.[51] The accurate charge of the supercapacitor is determined according to the equation:

$$Q = \frac{1}{v}\int I_{(V)}dV \qquad (1)$$

where v (mV/s) is the potential scan rates, and $I(v)$ is the applied current. The accurate charge of PANI/graphene supercapacitor is 245 times larger than that of graphene supercapacitor at the same scan rate of 10 mV/s. This indicates that the electrochemical performance is significantly improved after the deposition of pseudo-capacitive PANI.

Figure 4(d) shows the galvanostatic charge-discharge curves of the stretchable PANI/graphene supercapacitor measured between 0 and 0.8 V at different current densities. As discussed in the previous paragraph, the accurate charge increases hundred times after depositing pseudo-capacitive PANI onto the surface of the porous graphene. Therefore, it is reasonable to assume that most electrochemical capacitance in our device is resulted from the presence of PANI. The porous graphene provides the skeleton with high specific area, and mostly plays the role as current collector in our structure. The specific capacitance (C_m) can be calculated as follows:

$$C_m = \frac{C}{m} = \frac{I \times \Delta t}{\Delta V \times m} \qquad (2)$$

where C_m is the specific capacitance, I is charge/discharge current, Δt is the discharge time, ΔV is the potential range, and m denotes the total mass of PANI. Thus, the extracted specific capacitances are 261.24, 245.01, 187.5, 166.26 and 114.9 F/g at the current densities of 0.38, 0.75, 2.25, 3.75 and 7.5 A/g, respectively, as shown in Figure 4(e). The specific capacitance of our device is higher than that of the reported stretchable supercapacitor with buckling SWNT electrode[23] (50 F/g) or SWNT-on-Textile supercapacitor[22] (140 F/g) because of the presence of the pseudo-capacitive PANI. In addition, the specific capacitance of our device is also higher than that of flexible PANI/SWNT supercapacitor[44] (31.4 F/g).

The PANI/graphene supercapacitor was tested by galvanostatic charge/discharge for 1000 cycles at a constant current of 1 mA/cm^2. Figure 4(f) shows the charge/discharge cycling performance of one represented supercapacitor. With the increase of the number of charge/discharge cycles, the specific capacitance of the supercapacitor is slightly decreased, with the 89% capacitance retention after 1000 charge/discharge cycles. The calculated Coulombic efficiency η only lost ~5% after 1000 cycle charge-discharge. Conductive polymer usually suffers poor cyclic stability caused by the swelling and shrinking during the charge-discharge process.[18,52] Such good electrochemical stability achieved here for PANI should be attributed to that the dense PANI thin film was supported by porous graphene and sealed in robust and elastic solid-state gel electrolyte/Ecoflex, resulting in good protective effect on the PANI during swelling/shrinking.

Electrochemical impedance spectroscopy (EIS) of the supercapacitor was measured in the range of 0.1 Hz to 100 kHz in order to evaluate the kinetics as well as ionic resistance of the device. Figure 4(g) shows the Nyquist plot of the supercapacitor, and the inset of Figure 4(g) shows the plot with enlarged scale at high frequency range measurement. At low frequency region, the impedance characteristic is related to the diffusion of electrolyte ions into the active materials. The slope of the plot of our supercapacitor is close to 90°, indicating a predominantly capacitive behavior. At high frequency region, the low intercept at Z real axis (6.4 Ω) is related to the low equivalent series resistance (ESR) of the device. The energy density (E, Wh/kg), and the power density (P, W/kg) can be calculated by the following equations:

$$E = \frac{1}{2} \times C \times V^2 \qquad (3)$$

$$P = \frac{E}{t} = \frac{1}{2 \times m} \times I \times V \qquad (4)$$

where C is specific capacitance calculated by equation (2), V is the sweep potential window, and m is the mass of the total active materials. The power and energy density of the supercapacitor under different applied currents are shown in figure 4(h). The stretchable supercapacitor exhibits an energy density of 23.2 Wh/kg at a power density of 399 W/kg for a 0.8 V window voltage. It also preserves 44% of its energy density as the power density increases to 799 W/kg. The energy density of our device is better than those previously reported symmetrical PANI/SWNT[44] (7.1Wh/kg) and MnO_2/graphene supercapacitors (6.8 Wh/kg).[28] A rough comparison indicates that these values are compared with those of other similar flexible supercapacitors, such as, graphene/PANI nanofiber composite films[33] (15-19 Wh/kg) and supercapacitor based on PANI nanowire array encapsulated in titania nanotubes electrode (36.6 Wh/kg).[31]

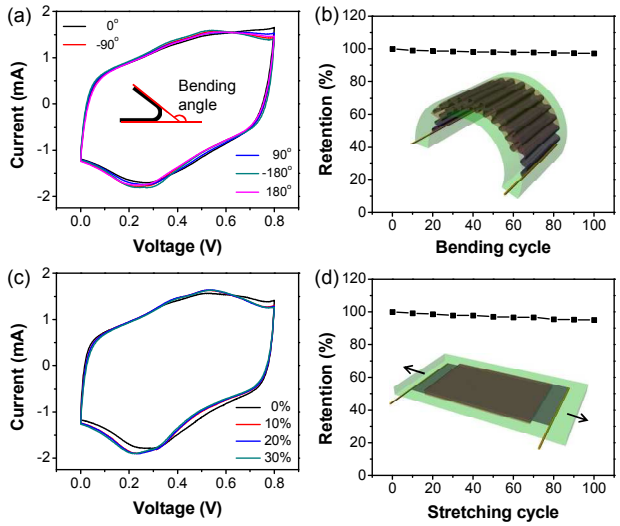

Figure 5. Electrochemical stability tests of the stretchable all-solid-state devices. (a) The CV curves of the stretchable supercapacitor with different bending status. (b) Bending (180°) cycle test of the supercapacitor. Inset is schematic of the supercapacitor in bending status. (c) The CV curves of the stretchable supercapacitor with different stretching status. (d) Stretching cycle test of the supercapacitor before and after different cycles of stretching to 20%. Inset is a schematic of the supercapacitor in a stretching state.

The wavy shaped PANI/graphene supercapacitor is not only bendable but also stretchable, as schematically shown in insets of Figure 5(c) and 5(d), respectively. The electrochemical properties of the stretchable supercapacitors were studied under different bending angles, bending cycles, different percentage of stretching, and stretching cycles. Figure 5(a) shows the CV curves of the PANI/graphene supercapacitor at different bending angles (from -180° to 180°). The CV curves under different bending states exhibit negligible differences, indicating that the electrochemical properties of the supercapacitor are less affected by large bending stress. Figure 5(b) shows the specific capacitance of the supercapacitor after bending from 0° (flat state) to 180° for different cycles. Our results show that 97% capacitance retention after 100 bending cycles. Figure 5(c) shows the CV curves of the supercapacitor under different applied tensile strain. It can be seen that the CV curves of the device show unobvious differences, revealing that the electrochemical performance of the stretchable supercapacitors remains unchanged even under 30% applied tensile strain. The electrochemical performance also shows excellent endurances under stretching cycles (Figure 5(d)). The stretching test of the supercapacitor shows 95% capacitance retention over 100 cycles. These electrochemical performances under different mechanical deformation reveal the excellent electrochemical and mechanical properties of the stretchable supercapacitor. These results clearly show that our stretchable all-solid-state supercapacitor, combining PANI/graphene composite electrode and with the wavy shape design, enables the device to be tolerate with large-scale mechanical deformation, while maintaining the excellent electrochemical performance.

4. Conclusions

We demonstrate a new kind of stretchable all-solid-state supercapacitor configuration with two slightly separated wavy shaped PANI/graphene electrodes and H_3PO_4-PVA gel electrolyte. To overcome the lack of stretchability of porous graphene, two porous graphene sheets in wavy shape were used as electrodes of supercapacitor. A dense pseudo-capacitive PANI thin film was conformally deposited onto porous graphene, increasing both the capacitance and the mechanical strength. The supercapacitor was encapsulated by elastomeric Ecoflex that can be stretched to a large scale. The supercapacitor exhibits a maximum specific capacitance of 261 F/g and an energy density of 23.2 Wh/kg at a power density of 399 W/kg for a 0.8 V window voltage. Our stretchable all-solid-state supercapacitor shows good electrochemical performance under maximum strain of 30%, and demonstrates a high potential as an energy storage device for stretchable and wearable electronic.

Acknowledgements

We acknowledge partial financial support from the Hong Kong Polytechnic University (Grant numbers: G-UA51and G-YN02), and the National Natural Science Foundation of China (Grant number: 61302045).

Notes and references

1. X. L. Hu, P. Krull, B. de Graff, K. Dowling, J. A. Rogers and W. J. Arora, *Adv Mater*, 2011, 23, 2933-2936.
2. R. H. Kim, H. Tao, T. I. Kim, Y. H. Zhang, S. Kim, B. Panilaitis, M. M. Yang, D. H. Kim, Y. H. Jung, B. H. Kim, Y. H. Li, Y. G. Huang, F. G. Omenetto and J. A. Rogers, *Small*, 2012, 8, 2812-2818.
3. R. H. Kim, D. H. Kim, J. L. Xiao, B. H. Kim, S. I. Park, B. Panilaitis, R. Ghaffari, J. M. Yao, M. Li, Z. J. Liu, V. Malyarchuk, D. G. Kim, A. P. Le, R. G. Nuzzo, D. L. Kaplan, F. G. Omenetto, Y. G. Huang, Z. Kang and J. A. Rogers, *Nat Mater*, 2010, 9, 929-937.
4. H. C. Ko, M. P. Stoykovich, J. Z. Song, V. Malyarchuk, W. M. Choi, C. J. Yu, J. B. Geddes, J. L. Xiao, S. D. Wang, Y. G. Huang and J. A. Rogers, *Nature*, 2008, 454, 748-753.
5. I. W. Jung, J. L. Xiao, V. Malyarchuk, C. F. Lu, M. Li, Z. J. Liu, J. Yoon, Y. G. Huang and J. A. Rogers, *P Natl Acad Sci USA*, 2011, 108, 1788-1793.
6. G. Shin, I. Jung, V. Malyarchuk, J. Z. Song, S. D. Wang, H. C. Ko, Y. G. Huang, J. S. Ha and J. A. Rogers, *Small*, 2010, 6, 851-856.
7. I. Jung, G. Shin, V. Malyarchuk, J. S. Ha and J. A. Rogers, *Appl Phys Lett*, 2010, 96.
8. J. Lee, J. A. Wu, M. X. Shi, J. Yoon, S. I. Park, M. Li, Z. J. Liu, Y. G. Huang and J. A. Rogers, *Adv Mater*, 2011, 23, 986-991.
9. D. J. Lipomi, B. C. K. Tee, M. Vosgueritchian and Z. Bao, *Adv Mater*, 2011, 23, 1771-1775.
10. D. H. Kim, N. S. Lu, R. Ma, Y. S. Kim, R. H. Kim, S. D. Wang, J. Wu, S. M. Won, H. Tao, A. Islam, K. J. Yu, T. I. Kim, R. Chowdhury, M. Ying, L. Z. Xu, M. Li, H. J. Chung, H. Keum, M. McCormick, P. Liu, Y. W. Zhang, F. G. Omenetto, Y. G. Huang, T. Coleman and J. A. Rogers, *Science*, 2011, 333, 838-843.
11. W.-H. Yeo, Y.-S. Kim, J. Lee, A. Ameen, L. Shi, M. Li, S. Wang, R. Ma, S. H. Jin, Z. Kang, Y. Huang and J. A. Rogers, *Adv Mater*, 2013, 25, 2773-2778.
12. T. Someya, T. Sekitani, S. Iba, Y. Kato, H. Kawaguchi and T. Sakurai, *P Natl Acad Sci USA*, 2004, 101, 9966-9970.
13. S. C. B. Mannsfeld, B. C. K. Tee, R. M. Stoltenberg, C. V. H. H. Chen, S. Barman, B. V. O. Muir, A. N. Sokolov, C. Reese and Z. N. Bao, *Nat Mater*, 2010, 9, 859-864.
14. K. Takei, T. Takahashi, J. C. Ho, H. Ko, A. G. Gillies, P. W. Leu, R. S. Fearing and A. Javey, *Nat Mater*, 2010, 9, 821-826.

15. Y. M. Song, Y. Z. Xie, V. Malyarchuk, J. L. Xiao, I. Jung, K. J. Choi, Z. J. Liu, H. Park, C. F. Lu, R. H. Kim, R. Li, K. B. Crozier, Y. G. Huang and J. A. Rogers, *Nature*, 2013, 497, 95-99.
16. N.-S. Choi, Z. Chen, S. A. Freunberger, X. Ji, Y.-K. Sun, K. Amine, G. Yushin, L. F. Nazar, J. Cho and P. G. Bruce, *Angewandte Chemie International Edition*, 2012, 51, 9994-10024.
17. Y. Huang, J. Liang and Y. Chen, *Small*, 2012, 8, 1805-1834.
18. K. Wang, H. Wu, Y. Meng and Z. Wei, *Small*, 2013, 10, 14-31.
19. Y. Wang and Y. Xia, *Adv Mater*, 2013, 25, 5336-5342.
20. Y. B. Tan and J.-M. Lee, Journal of Materials Chemistry A, 2013, 1, 14814-14843.
21. C. Yu, C. Masarapu, J. Rong, B. Wei and H. Jiang, *Adv Mater*, 2009, 21, 4793-4797.
22. L. Hu, M. Pasta, F. L. Mantia, L. Cui, S. Jeong, H. D. Deshazer, J. W. Choi, S. M. Han and Y. Cui, *Nano Letters*, 2010, 10, 708-714.
23. X. Li, T. Gu and B. Wei, *Nano Letters*, 2012, 12, 6366-6371.
24. Z. Q. Niu, H. B. Dong, B. W. Zhu, J. Z. Li, H. H. Hng, W. Y. Zhou, X. D. Chen and S. S. Xie, *Adv Mater*, 2013, 25, 1058-1064.
25. D. Kim, G. Shin, Y. J. Kang, W. Kim and J. S. Ha, ACS Nano, 2013, 7, 7975-7982.
26. L. L. Zhang and X. S. Zhao, *Chem Soc Rev*, 2009, 38, 2520-2531.
27. P. Simon and Y. Gogotsi, *Nat Mater*, 2008, 7, 845-854.
28. Y. He, W. Chen, X. Li, Z. Zhang, J. Fu, C. Zhao and E. Xie, *ACS Nano*, 2012, 7, 174-182.
29. W. Chen, Y. He, X. Li, J. Zhou, Z. Zhang, C. Zhao, C. Gong, S. Li, X. Pan and E. Xie, *Nanoscale*, 2013, 5, 11733-11741.
30. T. Chen, Y. Xue, A. K. Roy and L. Dai, ACS Nano, 2013, 8, 1039-1046.
31. K. Xie, J. Li, Y. Lai, Z. a. Zhang, Y. Liu, G. Zhang and H. Huang, *Nanoscale*, 2011, 3, 2202-2207.
32. M. A. Bavio, G. G. Acosta and T. Kessler, *Journal of Power Sources*, 2014, 245, 475-481.
33. Q. Wu, Y. Xu, Z. Yao, A. Liu and G. Shi, *ACS Nano*, 2010, 4, 1963-1970.
34. M. Sawangphruk, M. Suksomboon, K. Kongsupornsak, J. Khuntilo, P. Srimuk, Y. Sanguansak, P. Klunbud, P. Suktha and P. Chiochan, Journal of Materials Chemistry A, 2013, 1, 9630-9636.
35. J. Li, H. Xie, Y. Li, J. Liu and Z. Li, *Journal of Power Sources*, 2011, 196, 10775-10781.
36. Y.-Y. Horng, Y.-C. Lu, Y.-K. Hsu, C.-C. Chen, L.-C. Chen and K.-H. Chen, *Journal of Power Sources*, 2010, 195, 4418-4422.
37. Z. Yin and Q. Zheng, *Advanced Energy Materials*, 2012, 2, 179-218.
38. J. Benson, I. Kovalenko, S. Boukhalfa, D. Lashmore, M. Sanghadasa and G. Yushin, *Adv Mater*, 2013, 25, 6625–6632.
39. Z. P. Chen, W. C. Ren, L. B. Gao, B. L. Liu, S. F. Pei and H. M. Cheng, *Nat Mater*, 2011, 10, 424-428.
40. X. H. Cao, Y. M. Shi, W. H. Shi, G. Lu, X. Huang, Q. Y. Yan, Q. C. Zhang and H. Zhang, *Small*, 2011, 7, 3163-3168.
41. W. Wang, S. R. Guo, M. Penchev, I. Ruiz, K. N. Bozhilov, D. Yan, M. Ozkan and C. S. Ozkan, *Nano Energy*, 2013, 2, 294-303.
42. Y. Zhao, J. Liu, Y. Hu, H. H. Cheng, C. G. Hu, C. C. Jiang, L. Jiang, A. Y. Cao and L. T. Qu, Adv Mater, 2013, 25, 591-595.
43. *Y. Liu, Y. Ma, S. Guang, H. Xu and X. Su, Journal of Materials Chemistry A, 2014, 2, 813-823.*
44. C. Meng, C. Liu, L. Chen, C. Hu and S. Fan, *Nano Letters*, 2010, 10, 4025-4031.
45. Y. Wang, R. Yang, Z. Shi, L. Zhang, D. Shi, E. Wang and G. Zhang, *ACS Nano*, 2011, 5, 3645-3650.
46. X. Li, R. J. Zhang, W. J. Yu, K. L. Wang, J. Q. Wei, D. H. Wu, A. Y. Cao, Z. H. Li, Y. Cheng, Q. S. Zheng, R. S. Ruoff and H. W. Zhu, *Sci Rep-Uk*, 2012, 2.
47. M. Kaempgen, C. K. Chan, J. Ma, Y. Cui and G. Gruner, *Nano Letters*, 2009, 9, 1872-1876.
48. Z. Niu, L. Zhang, L. Liu, B. Zhu, H. Dong and X. Chen, *Adv Mater*, 2013, 25, 4035–4042.
49. L. D. Arsov, W. Plieth and G. Kossmehl, *J Solid State Electr*, 1998, 2, 355-361.
50. M. Tagowska, B. Pałys and K. Jackowska, *Synthetic Metals*, 2004, 142, 223-229.
51. Y. G. Wang, H. Q. Li and Y. Y. Xia, *Adv Mater*, 2006, 18, 2619-2623.
52. T. Kobayashi, H. Yoneyama and H. Tamura, *Journal of Electroanalytical Chemistry and Interfacial Electrochemistry*, 1984, 177, 281-291.